LEWIS GRANT

IN-39

48115

P. 26

NASA Contractor Report 187174

Probability of Brittle Failure

A. Kim
University of Illinois at Chicago
Chicago, Illinois

C.P. Bosnyak
Dow Chemical Company
Freeport, Texas

and

A. Chudnovsky
University of Illinois at Chicago
Chicago, Illinois

September 1991

NASA
National Aeronautics and
Space Administration

Introduction

The objective of the present project is to develop a methodology of fracture toughness characterization of ceramics on the basis of Crack Diffusion Model (CDM). The latter intends to explain the scatter of conventional fracture parameters and the "scale effect", i.e., dependence of fracture parameters on the specimen dimensions. CDM recognizes the presence of a random field of microinhomogeneities as the source of the scale effect and the scatter. Statistical parameters of the random field characterize the material and are independent of the specimen geometry. Their evaluation requires a data bank of either critical loads or critical crack lengths or crack penetration depths. The type of the specimens is not restricted by CDM, but is rather dictated by convenience of testing procedures.

For ceramics, such specimen types as single edge notched, bending, etc. used to evaluate critical quantities (load, stress intensity factor and so on) are undesirable. Indeed, the specimens are costly whereas each yields only one data point out of, say, twenty required for a statistically representative sample set. This motivated the choice of a compact tension specimen. The challenge became to achieve multiple crack initiations and arrests in a CT specimen made of ceramics (even single crack arrest was believed to be nearly impossible to obtain due to the rigidity of ceramics). Recently, after a year long effort, A. Calomino from NASA Lewis Research Center solved successfully this problem. In the meantime, the methodology of multiple crack initiation and arrest analysis has been tested on a model material (epoxy). Epoxy offers the convenience of specimen preparation and well detectable crack initiation and arrest positions. Our findings in this matter are presented below.

Background

Griffith's criterion, i.e. $G_1 = 2\gamma$, where G_1 is the energy release per unit crack advance (ERR) and γ is the surface (fracture) energy, is one of the most celebrated results in studies of brittle fracture. It expresses the necessary condition of stability (or instability) of a cracked solid with respect to crack extension. Particularly, it implies that the critical value of ERR at an arrest of a propagating crack, $G_1^{(a)}$, coincides with that at crack initiation, $G_1^{(i)}$, both being equal to 2γ.

However, experimental data on brittle crack formation in epoxides indicate that the values of $G_1^{(i)}$ may be significantly larger than those of $G_1^{(a)}$[1-5]. This difference depends on loading rate, temperature, crack propagation rate, chemical composition and curing conditions of the epoxy. The origin of the difference remains to be identified. In this paper a systematic energy analysis of crack initiation and arrest, quantification of the micromechanisms of this phenomena and a discussion on the origin of the difference between $G_1^{(i)}$ and $G_1^{(a)}$ are presented.

Material, specimen geometry and testing procedure

Two plaques of thickness 2.1 mm and 4.2 mm were prepared from a mixture of Dow Epoxy Resin 332 (a bisphenol A diglycidyl ether), Dow Epoxy 732 (a polyglycol extended diglycidyl ether) and Dow Epoxy Hardener 20 (a diethylene-triamine curing agent) cured under the same conditions, (room temperature, 48 hours). The weight ratios of DER 332:DER732:DEH 20 were 100:10:12.5. The Tg of the plaques were determined to be 61±2ºC using a Differential Scanning Calorimeter with a heating rate of 10ºC/minute from 25ºC to 200ºC.

Two sets of compact tension specimens (small and large with dimensions shown in Fig. 1) were machined from the plaques. The initial cracks were introduced by razor blades. The thickness of individual specimens is reported in Table 1 and 2.

Tension ramp tests were performed on an Instron 1330 servo-hydraulic test system at ambient conditions. All tests loadings were displacement controlled with a rate of 0.14 mm/min.
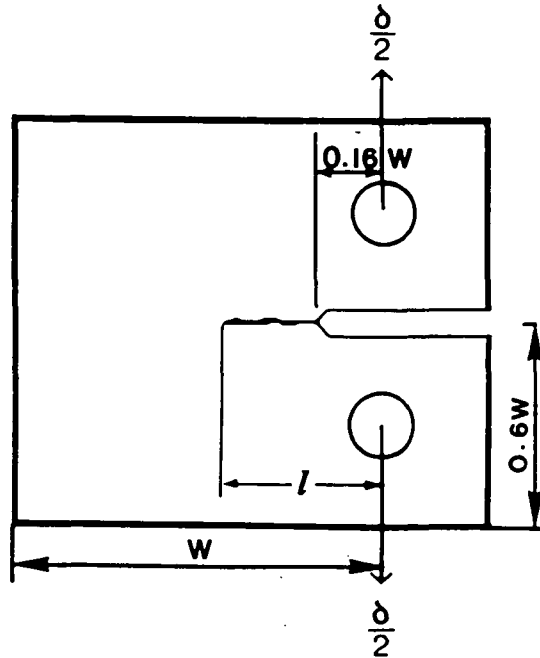

Figure 1   Specimen geometry and sizes; w = 25.6 mm and 45.0 mm for small and large specimens, respectively.

Results and Observations

Typically 4-5 crack initiations and subsequent arrests are gained from each specimen. Thus, just a few specimens supply a statistically representative set of data for analysis. A typical load-displacement curve is shown in Fig. 2. The load rises proportional to the increase in displacement to the first crack initiation point, 1^i. At this moment the crack rapidly advances, causing a sudden drop in the recorded load until the crack arrests at position 1^a. (Here, we employ the term "initiation" to indicate a transition from a steady crack or a slow quasi-static crack growth to a fast dynamic crack advance). As the displacement continues this process is subsequently repeated for a number of steps with crack initiations depicted at positions 2^i, 3^i, etc. and corresponding arrests at 2^a, 3^a, etc.. This phenomena is conventionally known as "stick-slip".
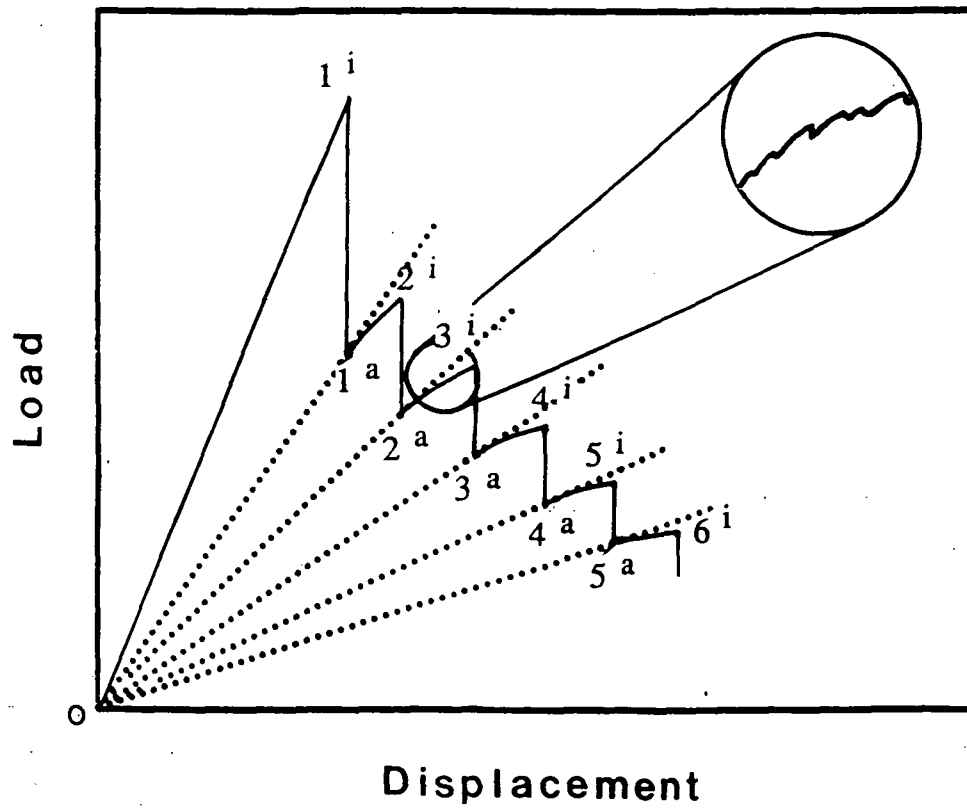
Figure 2   A typical load-displacement curve

The tangents of the load-displacement curves at the points 1^a, 2^a, ..., depicted by the dotted lines in Fig. 2, go through the origin, indicating a perfectly elastic response of the system immediately after crack arrest. On finer observation of the load-displacement curve on increasing displacement after crack arrest, shown in the enlargement of step 2^a-3^i, the curve deviates from linearity (i.e. an increase in compliance) and consists of smaller sharp drops of load resembling the larger steps. The increase in compliance indicates a sub-critical crack growth and the saw-tooth nature of this curve, shown in the enlargement, that this process procedes by discrete events. These suggestions are well supported by the morphology of the fracture surfaces.

Figure 3a shows a sketch of the fracture surface of specimen 2 observed by optical means. The dotted and solid lines indicate crack arrests and initiations, respectively. Triangles, or "deltoids", form between the arrest and initiation lines during sub-critical crack growth. The fact that the deltoids do not appear before the arrest line was established by rapid fracture of a specimen cooled in liquid nitrogen after the crack arrest. Figure 3b is an optical micrograph of the deltoid formations between the second arrest and third initiation events in specimen 2. These deltoid formations on the fractured surfaces are common for all specimens examined here and also can be seen in other studies[3,4]. The deltoids were further examined by scanning electron microscopy, SEM, after platinum coating the same specimens previously inspected by optical means. Figure 3c shows an SEM micrograph at 1000X of the region designated by the small box "B" in Fig. 3b. The deltoids appear on the scale of microns in height and 100 microns or larger in width and are complimentary on the two crack faces. The complimentarity, which has also been observed elsewhere[4], excludes any inelastic deformation from consideration. In other studies with epoxies prepared under various conditions some localized plastic shear deformation in the vicinity of the crack tip has been reported[1,2, 5]. However, Kinloch et. al[1,2] also reported the complimentarity of the fracture surface which should not be observed if plastic deformation occurs. It should also be noted that according to Phillips et al[4] the results of previous authors could not be reproduced (see p. 322 in ref. 4). The sub-micron scale texture of the fracture surface of the deltoid is similar to that of the crack jump after initiation and shows no indication of ductility.

DIRECTION OF CRACK

[a]

NOTCH

A

Arrest line

Initiation line

0.5 MM

B

2 ᵃ   3 ⁱ
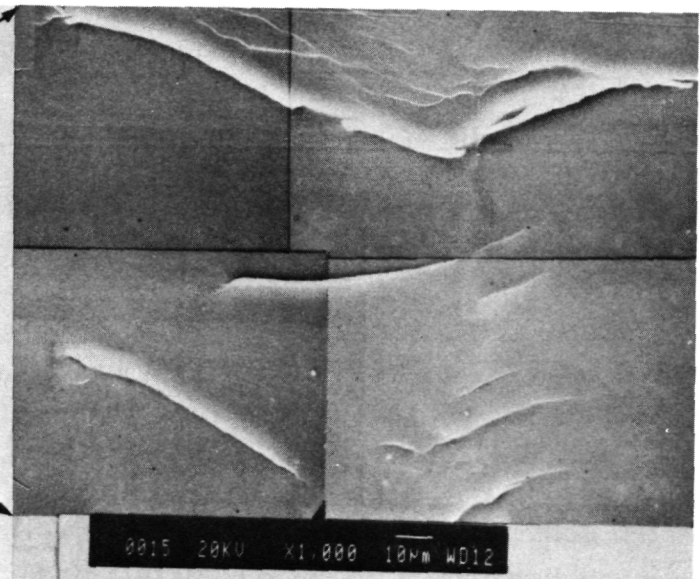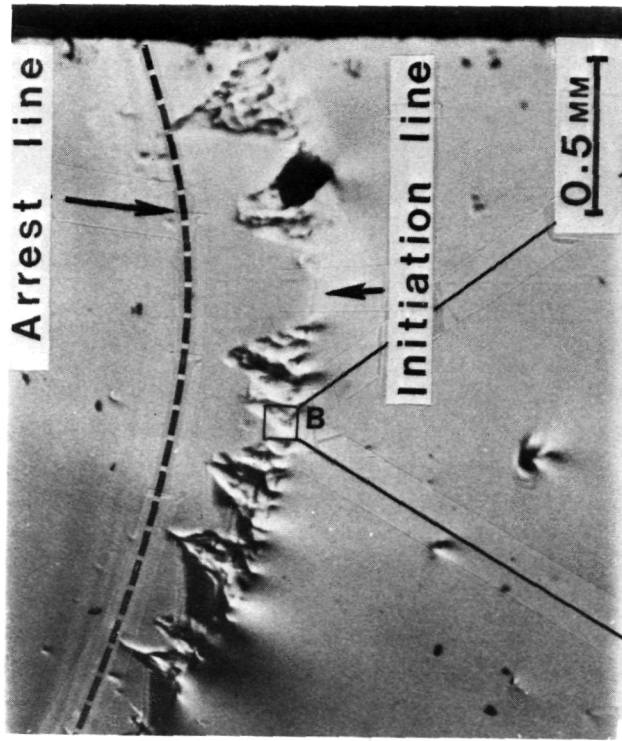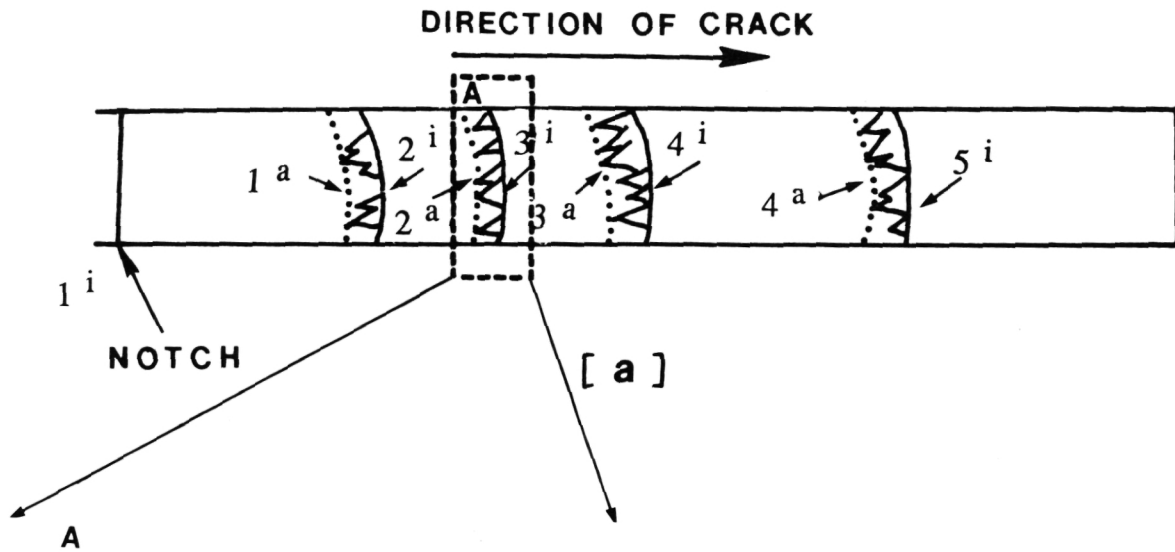
[b]   [c]

Figure 3a   A sketch of the fracture surface of specimen 2.
       3b   An optical micrograph of the deltoid formations between
            the second arrest and third initiation events in specimen 2
       3c   A SEM micrograph at 1000X of the region designated by
            the small box "B" in Fig. 3a.

Figures 4a and b show representative optical micrographs of the sub-critical crack growth zones of a small and large specimen, respectively, at the same magnification. The deltoid formations appear as a cascade of elementary deltoids with their bases extending in the direction of crack growth. The size of an elementary deltoid clearly appears to be invariant with respect to specimen thickness and also with the steps 1^a-2^i, 2^a-3^i, etc. Thus, it appears that the discontinuous nature of the sub-critical crack advance recorded in the load-displacement curves is related to the deltoids observed on the fracture surface.
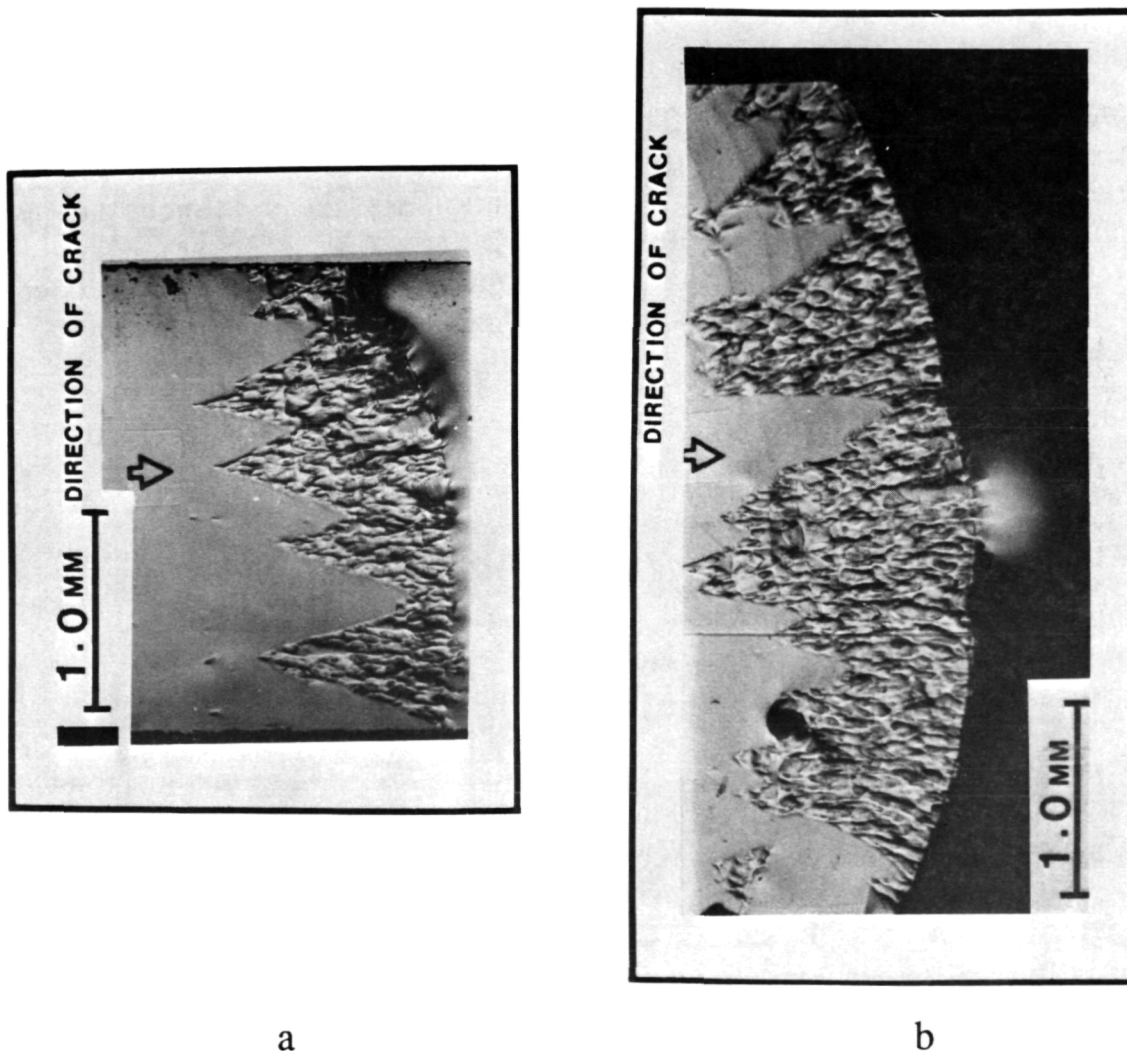

a   b

Figure 4   Optical micrographs of the cascades of deltoids of a small [a] and large specimen [b], at the same magnification.

Discussion

The energy release rates at initiation, $G_1^{(i)}$, and arrest, $G_1^{(a)}$, as well as the total energy released on sub-critical growth, can be readily evaluated based on the elastic solution (Appendix 1). The values of the energy release rates $G_1^{(i)}$ and $G_1^{(a)}$ for specimens 1 and 2 are given in Figs. 5 and 6. Also shown are the corresponding fracture surfaces between the crack arrest and initiation lines. Typically, the values for $G_1^{(a)}$ for all the specimens are fairly constant and significantly smaller than those for $G_1^{(i)}$. The values of $G_1^{(i)}$ change randomly with crack length. Analogous findings have been reported by Phillips *et al*[4]. The data necessary for ERR evaluation for the specimens studied here are summarized in Tables 1 and 2.

It is our observation that the ERR at initiation is strongly correlated with the number N of deltoids in the last row of deltoid cascades, before initiation of the crack jump, as shown in Fig. 7. The intersection of a linear regression of $G_1^{(i)}$ as a function of N, in the limit of N approaching zero, falls within the range of $G_1^{(a)}$ (0.16 KJ/m^{2}) in agreement with Griffith's criterion. The tendency of $G_1^{(i)}$ to approach $G_1^{(a)}$ with increase in rate of loading as well as decrease of temperature have also been observed[1,2,4-6].

It is expected that the larger the difference $G_1^{(i)} - G_1^{(a)}$ i.e. the larger the excess of energy release rate at initiation over that at arrest, the larger the subsequent crack jump. An estimation of the crack jump, Δl, can be readily obtained within the framework of linear-elastic fracture mechanics. It should be noted that the crack jump after the initiation 1^i-1^a, 2^i-2^a, etc.,(Fig 2) is a faster process than the response of the actuator of the loading system. Thus the displacement, δ_i, at crack initiation remains practically constant during the crack jump from l_i to $l_i + \Delta l$. After the jump, the crack

Figure 5   Energy release rate at crack arrest and initiation vs. normalized crack length, l/w, and the micrographs of the fracture surface between the corresponding arrest and initiation lines of specimen
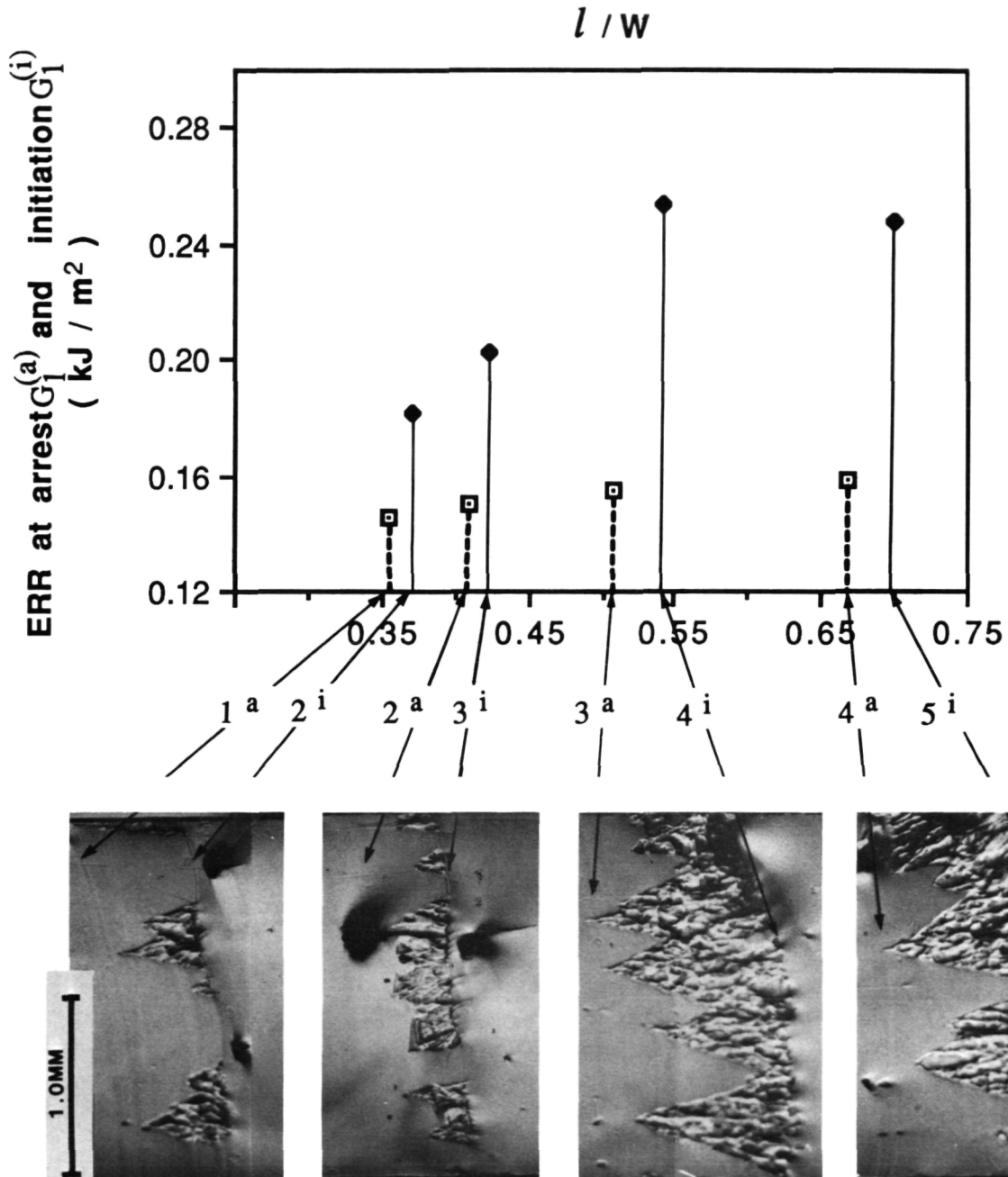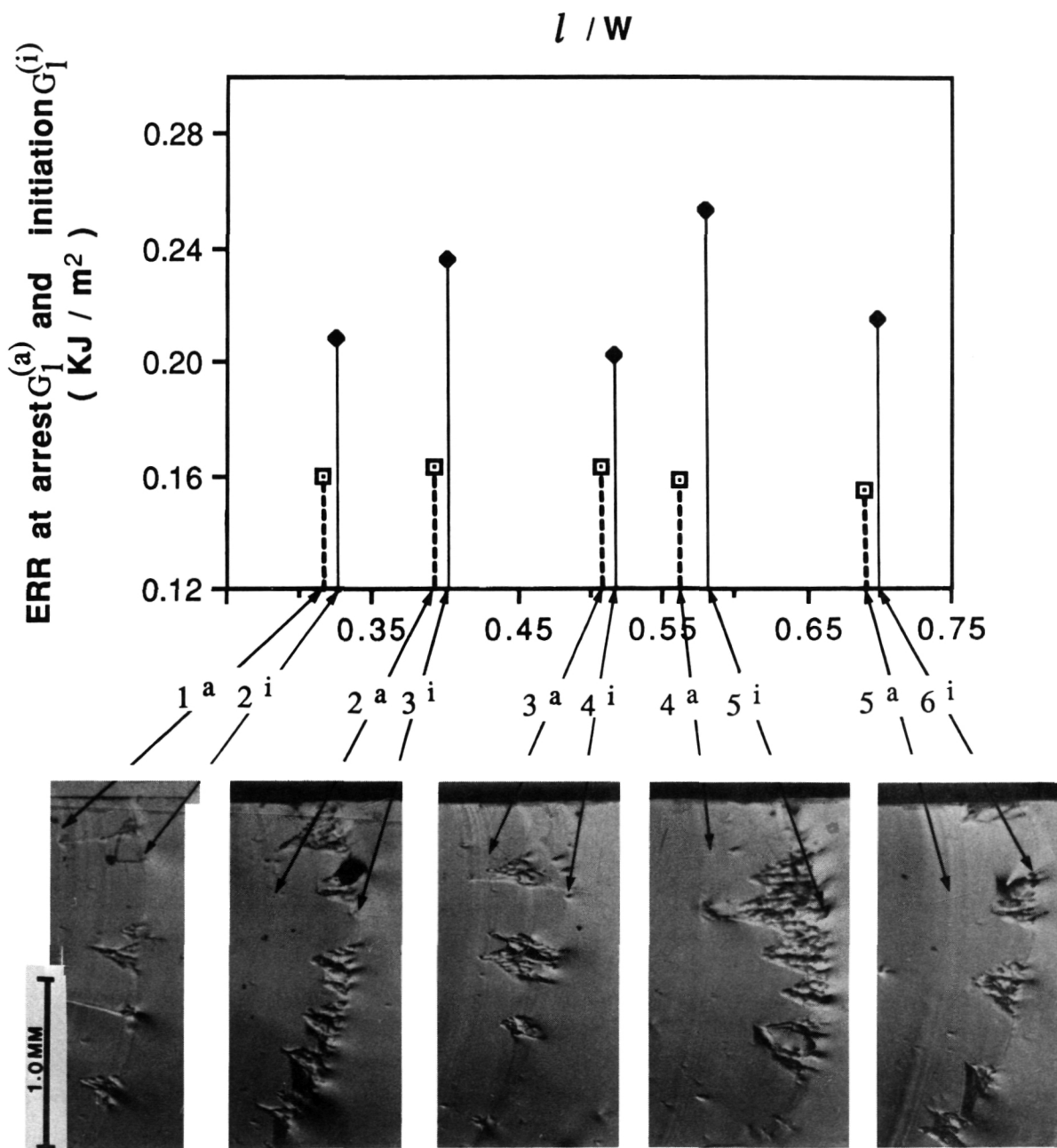
Figure 6   Energy release rate at crack arrest and initiation vs. normalized crack length, l/w, and the micrographs of the fracture surface between the corresponding arrest and initiation lines of specimen 2.

Table 1   Small specimen

Specimen NO.	Crack Advance Number	Crack Length (mm)		Load (N)		Total NO. of Δ's n_k^{tot}	NO of the last Δ's n_k^{last}	Thickness (mm)
		Initiation ℓ_k^i	Arrest ℓ_k^a	Initiation P_k^i	Arrest P_k^a			
1	1		9.06		33.81	24	13	
	2	9.52	10.47	36.25	29.80	39	17	
	3	10.83	12.98	33.36	22.91	91	26	2.16
	4	13.90	17.10	26.02	12.46	75	23	
	5	17.89		13.35				
2	1		8.06		38.70	10	8	
	2	8.29	10.06	43.15	32.03	24	17	
	3	10.29	12.98	37.59	23.13	10	7	2.13
	4	13.21	14.34	25.13	19.13	39	19	
	5	14.80	17.66	22.69	10.90	16	13	
	6	17.89		12.23				
3	1		10.27		31.58	18	12	
	2	10.50	12.34	35.14	25.13	19	14	
	3	12.70	14.85	28.69	17.79	20	12	2.13
	4	15.21	17.66	20.02	11.34	37	17	
	5	18.20		12.23				

Table 2   Large specimen

Specimen NO.	Crack Advance Number	Crack Length (mm)		Load (N)		Total NO. of Δ's n_k^{tot}	NO of the last Δ's n_k^{last}	Thickness (mm)
		Initiation ℓ_k^i	Arrest ℓ_k^a	Initiation P_k^i	Arrest P_k^a			
4	1		36.25		14.23	18	13	
	2	36.46		15.57				4.38
5	1		25.12		52.04	25	20	
	2	25.34	27.55	55.60	42.93	26	20	
	3	27.76	29.92	48.49	34.25	24	20	
	4	30.14	31.94	37.37	25.80	19	16	4.34
	5	32.16	33.92	27.80	19.79	22	17	
	6	34.13		21.13				
6	1		21.63		63.83	17	12	
	2	21.84	23.91	68.28	54.94	26	19	
	3	24.13	26.52	59.61	44.26	23	16	
	4	26.73	28.94	47.15	36.25	21	16	4.10
	5	29.15	31.05	38.70	27.80	9	7	
	6	31.26		29.58				

arrest takes place when the current energy release rate is reduced to the value at arrest, $G_1^{(a)}$. This can be expressed as follows:

$$G_1(l_i + \Delta l, \delta_i) = G_1^{(a)} \tag{1}$$

The LHS of the equation 1 can be expanded into a Taylor series

$$G_1(l_i + \Delta l, \delta_i) = G_1(l_i, \delta_i) + \frac{\partial G_1}{\partial l} \Big|_{l_i, \delta_i} \Delta l + \frac{1}{2} \frac{\partial^2 G_1}{\partial l^2} \Big|_{l_i, \delta_i} \Delta l^2 + \ldots \tag{2}$$

Neglecting the omitted higher order terms in the equation 2 and taking into consideration the equation 1 and the condition of crack initiation, $G_1(l_i, \delta_i) = G_1^{(i)}$, one obtains the following quadratic equation for Δl:

$$\frac{1}{2} \frac{\partial^2 G_1}{\partial l^2} \Big|_{l_i, \delta_i} \Delta l^2 + \frac{\partial G_1}{\partial l} \Big|_{l_i, \delta_i} \Delta l + G_1^{(i)} - G_1^{(a)} = 0 \tag{3}$$

The solution of the equation 3 normalized by the specimen width, W, is shown in Fig. 8 as a function of the normalized crack length, l/W. The dotted lines represent the upper and lower limits of the crack advance corresponding to the minimal and maximal values of $(G_1^{(i)} - G_1^{(a)})/ G_1^{(i)}$. The solid line in Fig.8 discribes the solution of the equation 3 for the average value of $(G_1^{(i)} - G_1^{(a)})/ G_1^{(i)}$. Figure 8 shows that the experimental data points are all within the band expected from the elastic solution. The scatter of the data in the band apparently reflects a mechanism controlled by chance.

Utilizing the same elastic solution we estimate the total potential energy release, $\Delta \Pi$, due to sub-critical crack advance (Appendix 2). A new surface area created during this process is $\Delta l \cdot t$ (t is the specimen thickness) and the part of this area, $N \cdot A^D$, is occupied by a cascade of deltoids (A^D is the elementary deltoid area and N is the total number of deltoids in cascade). Thus an excess of $\Delta \Pi$ over $2\gamma_0 \cdot \Delta l \cdot t$ can be attributed to the formation of deltoids:
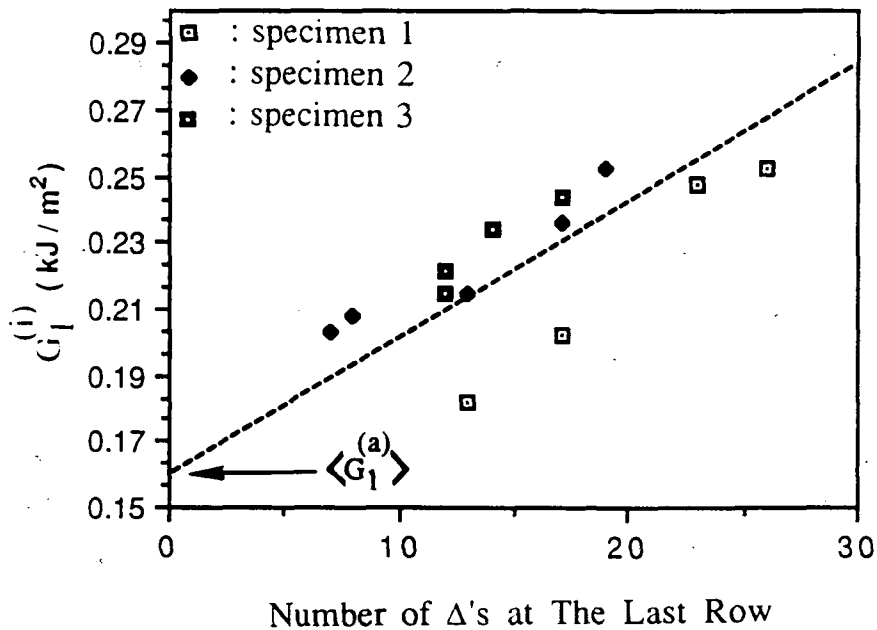
Figure 7   Energy release rate at initiation vs. No. of deltoids in the
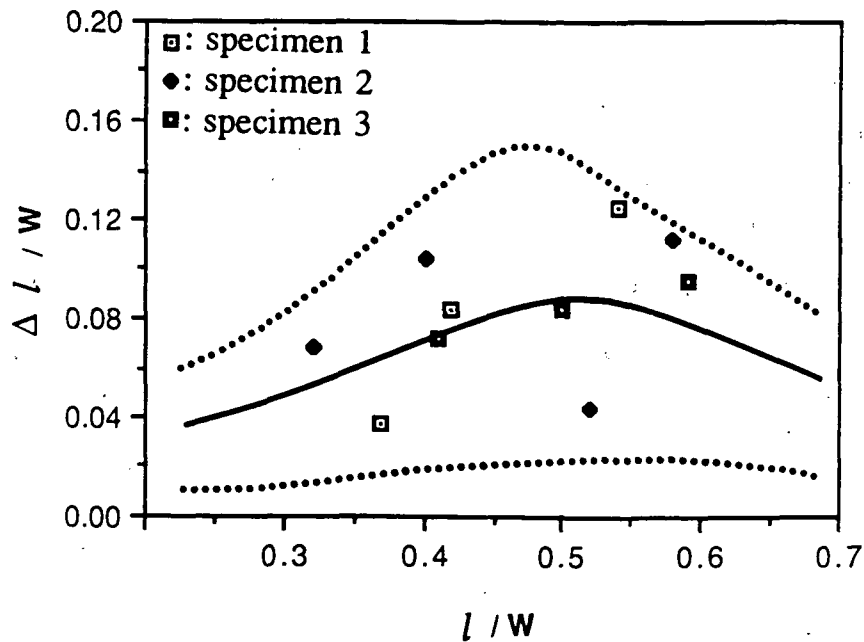last row of the corresponding cascade.

Figure 8   The normalized crack advance $\Delta l/w$ between the
initiation and the following arrest line vs. l/w. The solid
and dotted lines represent average minimal and maximal
values, repectively. The data points are observed values.

$$\Delta\Pi - 2\gamma_0 \cdot \Delta l \cdot t = 2(\gamma^D - \gamma_0) N \cdot A^D \qquad (4)$$

Here $2\gamma_0 = G_1^{(a)}$ stands for the specific fracture energy (SFE) for a smooth fracture surface and $2\gamma^D$ reflects the SFE for a fracture surface of deltoids. Figure 9 is a graphical representation of the equation 4 normalized by the crack advance area, $\Delta l \cdot t$; specifically it shows the potential energy release per unit area of sub-critical crack advance vs. the normalized deltoids area, $(N \cdot A^D)/(\Delta l \cdot t)$.

The dashed line represents a linear regression of all the data points with a fixed intersection at the average value of the ERR at crack arrest.

The intersection corresponds to $G_1^{(a)}$ and the slope reflects the excess of $2\gamma^D$ over $2\gamma_0$. The average of the deltoid SFE, $<2\gamma^D>$, is 0.261 KJ/m² and the standard deviation is 0.031 KJ/m².
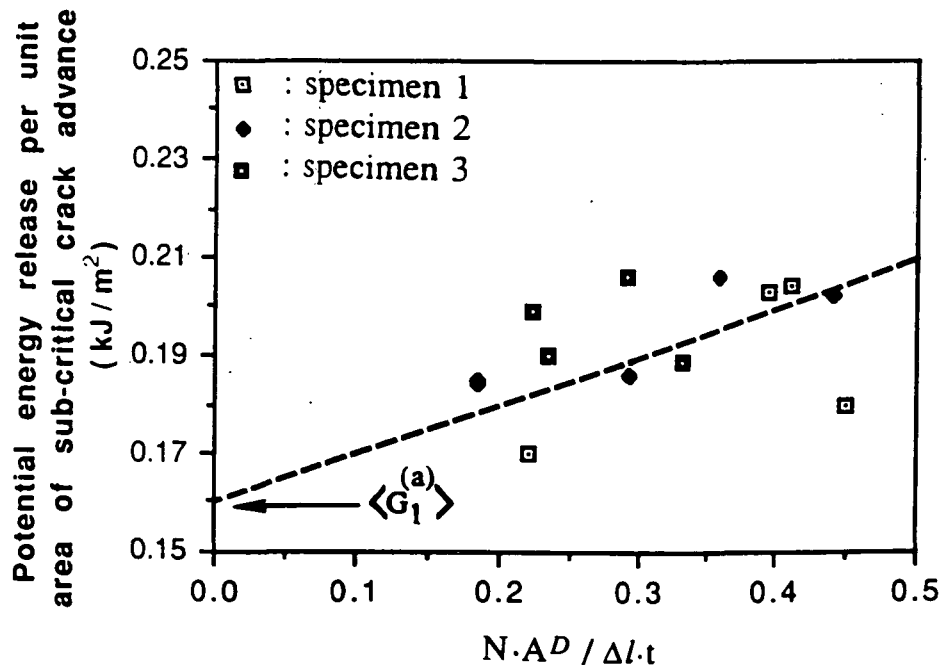This excess of energy may be associated with kinetic, heat and/or other forms of energy.

Figure 9   The potential energy release per unit area of sub-critical crack advance vs. the normalized deltoids area, $N \cdot A^D / \Delta l \cdot t$.

From the observations, the creation of the deltoids appears to be controlled by chance, which results in a large scatter of $G_1^{(i)}$. The difference between the fluctuating $G_1^{(i)}$ and relatively constant $G_1^{(a)}$ i.e. ΔG_1 is evaluated for the small and large specimens. The results reveal a strong scale effect, depicted in Fig. 10 which shows the distributions of ΔG_1 fitted by gamma distribution.

The scale effect resembles that expected for strength of a material controlled by the largest defects. This resemblance, together with the characteristic appearance of the apex of the deltoids, depicted in Fig. 4, are strongly suggestive of an underlying defect population as a primary source for the observed phenomena. Indeed, the deltoids are analogous to those created on a river surface downstream from a small obstacle.

However, in spite of our expectation based on this analogy and the observed scale effect, there are no "defects" at the apex of the deltoids detectable down to the 0.1 micron level. Moreover, the arrest and initiation lines do not correlate with apparent large-scale defects such as bubbles. This suggests that the formation of deltoids during the slow process of sub-critical crack growth is an intrinsic feature of the fracture process itself. It may be triggered by inhomogeneity of the epoxy. The inhomogeneity could be related for instance to a fluctuation in the cross-link density. A number of studies on epoxies have reported nodular structures or chemical crosslink density fluctuations which could arise out of inadequate mixing of the highly viscous components[5,7-9]. The relationship among the scale of structural inhomogeneity, the loading history and the micromechanisms of failure would thus be important to uncover.
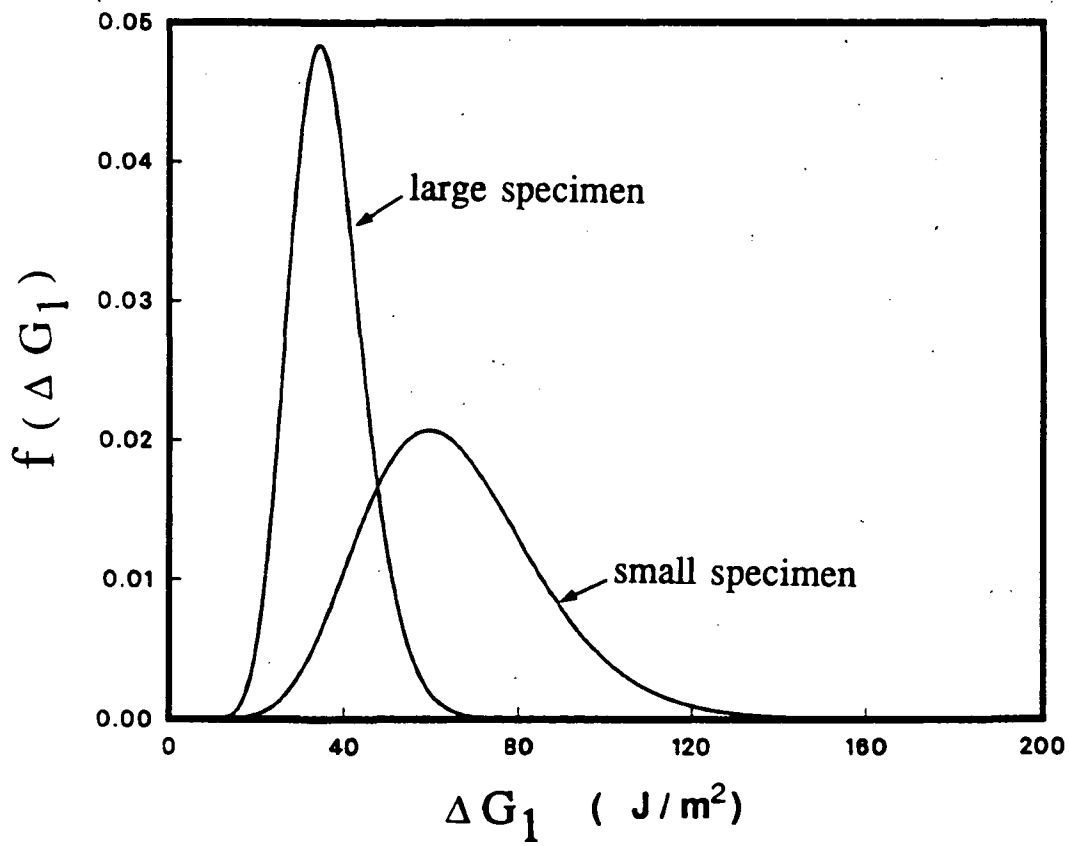
Figure 10   Distribution of $\Delta G_1 = G_1^{(i)} - G_1^{(a)}$ fitted by Gamma distribution for small and large specimens.

Conclusion

1. Four-five crack initiations and arrests are gained from each specimen. Thus following the experimental procedure described in this study, three specimens supply a statistically representative data.
2. The deltoids are formed on the fracture surface during the slow sub-critical crack growth, prior to the smooth mirror-like surface of the fast crack. The two faces of the fracture surface are complimentary which excludes any inelastic defomation.
3. The values of ERR at arrest are fairly constant and significantly smaller than those at initiation.
4. The values of ERR at initiation display random scatter and strong correlation with the number of deltoids in the last row of deltoid cascades.
5. There is a well pronounced scale effect in ERR at initiation. It resembles that in conventional strength of a material controlled by the largest defects, though no defects are found at deltoid apexes.

Acknowledgements

Appendix 1

The Stress Intensity Factor (SIF) for CT specimens shown in Fig. 1 is evaluated as follows(ASTM 399-81[10]) :

$$\text{S.I.F. } K_1 = \frac{\delta E'}{V(\xi)\sqrt{w}} \frac{(2+\xi)(0.866+4.64\xi-13.32\xi^2+14.72\xi^3-5.60\xi^4)}{(1-\xi)^{\frac{3}{2}}} \qquad \text{A-1.1}$$

where[11]

$$V(\xi) = \frac{1.277+15.45\xi+1.33\sin(2\Pi\xi)}{(1-\xi)^2} \qquad \text{for } 0.2 \leq \xi \leq 0.8 \qquad \text{A-1.2}$$

and $\xi = l/w$. The effective Young's modulus can be directly evaluated from the load-displacement curves such as shown in Fig. 2. Then the energy release rate $G_1 = K_1^2/E'$ can be readily evaluated as a function of the crack length l and the load point displacement (LPD), δ. The dependency of G_1 on the normalized crack length $\xi = l/w$ for different LPD, δ, is shown in Fig. 11.
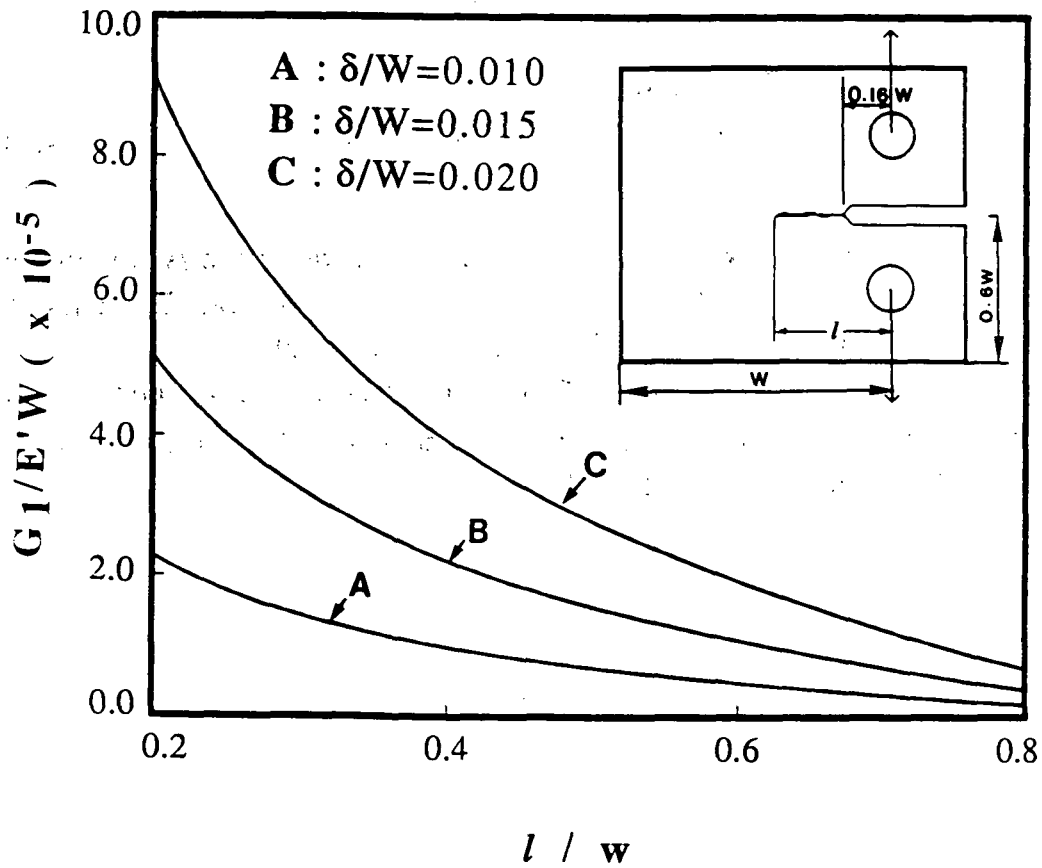
Figure 11   A family of normalized ERR vs. normalized crack length,
            l/w, parameterized by the normalized load-point
            displacement, δ/w.

Appendix 2

The evaluation of total potential energy change due to sub-critical crack growth can be done as following:

Since the potential energy $\Pi(P, l)$ or $\Pi(P, \delta)$ has two independent variables, the differential of Π is determined by:

$$d\Pi = \frac{\partial\Pi}{\partial l}dl + \frac{\partial\Pi}{\partial P}dP$$

If we approximate $\delta=\delta(P)$ from the experimental results, then the elastic equilibrial crack l (P, δ) becomes a function of P only. Therefore

$$dl = \frac{dl}{dP}dP \qquad\qquad\qquad\qquad\qquad\qquad \text{A-2.1}$$

and consequently A-2.1 becomes

$$d\Pi = \left(\frac{\partial\Pi}{\partial l}\frac{dl}{dP} + \frac{\partial\Pi}{\partial P}\right)dP \qquad\qquad\qquad\qquad \text{A-2.2}$$

where

$$\frac{\partial\Pi}{\partial l} = -G_1 \quad , \quad \frac{\partial\Pi}{\partial P} = -\frac{1}{2}\delta \quad ; \quad G_1 = G_1 \text{ x (specimen thickness)} \quad \text{A-2.3}$$

If one approximates $\delta=\delta(P)$ by a parabolic function

$$\delta = \delta_k + A(P-P_k^a) - B(P-P_k^a)^2 \qquad\qquad\qquad\qquad \text{A-2.4}$$

where A and B are constants and can be determined with such conditions:

$$\frac{d\delta}{dP}\Big|_{P=P_k^a} = C(l_k^a) \quad ; \quad C(l_k^a) \text{ stands for the compliance}$$

$$\delta_{k+1} = \delta_k + A(P_{k+1}^i - P_k^a) - B(P_{k+1}^i - P_k^a)^2$$

After the calculation

$$A = C(l_k^a) , \quad B = \frac{C(l_k^a)}{P_{k+1}^i - P_k^a} - \frac{\delta_{k+1} - \delta_k}{(P_{k+1}^i - P_k^a)^2}$$

A-2.5

From A-2.2 and A-2.3, the total potential energy change

$$\Delta\Pi = \int_{P_k^a}^{P_{k+1}^i} \left[-G_1\{l(P),P\}\frac{dl}{dP} - \frac{1}{2}\delta(P) \right]dP$$

A-2.6

The first term of A-2.6

$$\int_{P_k^a}^{P_{k+1}^i} \left[-G_1\{l(P),P\}\frac{dl}{dP} \right]dP = -G_1\{l(P),P\}l(P) \Big|_{P_k^a}^{P_{k+1}^i} + \int_{P_k^a}^{P_{k+1}^i} l(P)\frac{dG_1\{l(P),P\}}{dP}dP$$

$$\cong \frac{1}{2}(G_{1k+1}^{(i)} + G_{1k}^{(a)})(l_{k+1}^i - l_k^a)$$

A-2.7

The second term of A-2.6

$$\int_{P_k^a}^{P_{k+1}^i} \left[-\frac{1}{2}\delta(P) \right]dP = -\frac{1}{2}\int_{P_k^a}^{P_{k+1}^i} C\{l(P)\}PdP + \frac{1}{2}B\int_{P_k^a}^{P_{k+1}^i} (P-P_k^a)^2 dP$$

$$\cong \frac{(P_{k+1}^i - P_k^a)}{2}\left[-\frac{\{C(l_{k+1}^i) + C(l_k^a)\}(P_{k+1}^i + P_k^a)}{4} + \frac{1}{3}\{C(l_k^a)(P_{k+1}^i - P_k^a) - (\delta_{k+1} - \delta_k)\} \right]$$

A-2.8

Thus Eq. (A-2.6) = Eq. (A-2.7) + Eq. (A-2.8)

and $\Delta\Pi$ is expressed through observed quantities as

$$P_k^a , P_{k+1}^i , \delta_k , \delta_{k+1} , G_{1k}^{(a)} , G_{1k+1}^{(i)} , C(l_k^a) , C(l_{k+1}^i) , l_k^a , l_{k+1}^i$$

For the values of parameters under consideration the first term is about 95% of $\Delta\Pi$. Therefore the total potential energy change can be approximated as follows:

$$\Delta\Pi \cong \frac{1}{2}(G^{(i)}_{1k+1}+G^{(i)}_{1k})(l^{i}_{k+1}-l^{a}_{k})$$

References

1   R.A. Gledhill, A.J. Kinloch, S. Yamini and R.J. Young, *Polymer* 19 (1978) 574-581.

2   R. A. Gledhill and A.J. Kinloch, *Journal of Materials Science* 10 (1975) 1261.

3   A.J. Kinloch, Microstructure and Fracture Behavior, Rubber-Toughened Plastics, C.K. Riew, Ed., *Advances in Chemistry Series 222*, American Chemical Society, Washington, DC (1989) 71

4   D.C. Phillips, J.M. Scott and M. Jones, *Journal of Materials Science* 13 (1978) 311-322

5   J.D. LeMay and F.N. Kelley, Structure and Ultimate Properties of Epoxy Resins, *Advances in Polymer Science* , Springer-Verlag, Berlin, Heidelburg 78 (1986) 116-148.

6   V.-T. Truong, *Polymer,* 31 (1990) 1669-1677

7   R.J. Morgan, Structure-property relations of epoxies used as composite matrices, *Advances in Polymer Science* , Springer-Verlag, Berlin, Heidelburg 72 (1980) 1-43.

8   P.J. Aspbury and W.C. Wake, *British Polymer Journal* 11 (1979) 17-27

9   G. Levita, Matrix ductility and toughening of epoxy resins, Rubber-Toughened Plastics, C.K. Riew, Ed., *Advances in Chemistry Series 222,* American Chemical Society, Washington, DC (1989) 93-118

10   Standard Method of Test for Plane-Strain Fracture Toughness of Metallic Material, ASTM 399-81, *ASTM Annual Standards* Part 10.

11   T. Hiroshi, *The Stress Analysis of Cracks Handbook,* Del Research Corporation, St. Louis, Missouri (1973) 2.20-2.21

REPORT DOCUMENTATION PAGE

Public reporting burden for this collection of information is estimated to average 1 hour per response, including the time for reviewing instructions, searching existing data sources, gathering and maintaining the data needed, and completing and reviewing the collection of information. Send comments regarding this burden estimate or any other aspect of this collection of information, including suggestions for reducing this burden, to Washington Headquarters Services, Directorate for Information Operations and Reports, 1215 Jefferson Davis Highway, Suite 1204, Arlington, VA 22202-4302, and to the Office of Management and Budget, Paperwork Reduction Project (0704-0188), Washington, DC 20503.

1. AGENCY USE ONLY (Leave blank)	2. REPORT DATE	3. REPORT TYPE AND DATES COVERED
	September 1991	Final Contractor Report

4. TITLE AND SUBTITLE	5. FUNDING NUMBERS
Probability of Brittle Failure	WU-505-63-40
6. AUTHOR(S)	G-NAG3-1034
A. Kim, C.P. Bosnyak, and A. Chudnovsky	

7. PERFORMING ORGANIZATION NAME(S) AND ADDRESS(ES)	8. PERFORMING ORGANIZATION REPORT NUMBER
University of Illinois at Chicago Department of Civil Engineering, Mechanics, and Metallurgy Chicago, Illinois 60680	None

9. SPONSORING/MONITORING AGENCY NAMES(S) AND ADDRESS(ES)	10. SPONSORING/MONITORING AGENCY REPORT NUMBER
National Aeronautics and Space Administration Lewis Research Center Cleveland, Ohio 44135-3191	NASA CR-187174

11. SUPPLEMENTARY NOTES

Project Manager, John P. Gyekenyesi, Structures Division, NASA Lewis Research Center, (216) 433-3210. A. Kim and A. Chudnovsky, University of Illinois at Chicago; C.P. Bosnyak, Dow Chemical Company, Polycarbonate R&D, B-1470, Highway 227, Freeport, Texas 77541.

12a. DISTRIBUTION/AVAILABILITY STATEMENT	12b. DISTRIBUTION CODE
Unclassified - Unlimited Subject Category 39	

13. ABSTRACT (Maximum 200 words)

The objective of this work is to develop a methodology for collecting statistically representative data for crack initiation and arrest from small number of test specimens. An epoxy (based on bisphenol A diglycidyl ether and polyglycol extended diglycidyl ether and cured with diethylene triamine) is selected as a model material. A compact tension specimen with displacement-controlled loading is employed to observe multiple crack initiations and arrests. The energy release rate at crack initiation is significantly higher than that at crack arrest, as has been observed elsewhere. In this study the difference between these energy release rates is found to depend on specimen size (scale effect), and is quantitatively related to the fracture surface morphology. The scale effect, similar to that in statistical strength theory, is conventionally attributed to the statistics of defects which control the fracture process. Triangular shaped ripples (deltoids) are formed on the fracture surface during the slow subcritical crack growth, prior to the smooth mirror-like surface characteristic of fast cracks. The deltoids are complimentary on the two crack faces which excludes any inelastic deformation from consideration. The deltoids are analogous to the ripples created on a river surface downstream from a small obstacle. Presence of defects is also suggested by the observed scale effect. However, there are no "defects" at the deltoid apexes detectable down to the 0.1 micron level. This indicates that the formation of deltoids during the slow process of sub-critical crack growth is an intrinsic feature of the fracture process itself, possibly triggered by inhomogeneity of material on a sub-micron scale.

14. SUBJECT TERMS			15. NUMBER OF PAGES
Crack initiation; Crack arrest; Crack propagation; Fracture strength			26
			16. PRICE CODE A03

17. SECURITY CLASSIFICATION OF REPORT	18. SECURITY CLASSIFICATION OF THIS PAGE	19. SECURITY CLASSIFICATION OF ABSTRACT	20. LIMITATION OF ABSTRACT
Unclassified	Unclassified	Unclassified	

National Aeronautics and
Space Administration

Lewis Research Center
Cleveland, Ohio 44135

FOURTH CLASS MAIL

ADDRESS CORRECTION REQUESTED

NASA